

An antisense RNA capable of modulating the expression of the tumor suppressor microRNA-34a

Jason T. Serviss^{1*}, Felix Clemens Richter^{1,2}, Jimmy Van Den Eynden³, Nathanael Johansson Andrews¹, Miranda Houtman^{1,4}, Laura Schwarzmueller^{1,5}, Per Johnsson, Erik Larsson³, Dan Grandér¹, Katja Pokrovskaia Tamm¹

¹ Department of Oncology and Pathology, Karolinska Institutet, Stockholm, Sweden, SE-17177

² Kennedy Institute of Rheumatology, University of Oxford, Roosevelt Drive, Oxford OX3 7FY, UK

³ Department of Medical Biochemistry and Cell Biology, Institute of Biomedicine, The Sahlgrenska Academy, University of Gothenburg, SE-405 30 Gothenburg, Sweden

⁴ Rheumatology Unit, Department of Medicine, Karolinska University Hospital Solna, Karolinska Institutet, Stockholm, Sweden

⁵ Laboratory for Experimental Oncology and Radiobiology (LEXOR), Center for Experimental Molecular Medicine (CEMM), Academic Medical Center, Amsterdam, The Netherlands

*** Correspondence:**

Jason T. Serviss jason.serviss@ki.se

Abstract

The microRNA-34a is a well-studied tumor suppressor microRNA (miRNA) that is a direct downstream target of TP53 and has roles in multiple pathways associated with oncogenesis, such as proliferation, cellular growth, and differentiation. Due to its wide variety of targets that suppress oncogenesis, it is not surprising that *miR34a* expression has been shown to be dysregulated in a wide variety of solid tumors and hematological malignancies. Despite this, the mechanisms by which *miR34a* is regulated in these cancers is not well studied. In this study, we find that a long non-coding RNA transcribed antisense to *miR34a* host gene, is critical for *miR34a* expression and mediation of its cellular functions in multiple types of human cancer. In addition, we characterize *miR34a* antisense RNA's ability to facilitate *miR34a*

39 expression under multiple types of cellular stress in both *TP53* deficient and
40 wildtype settings.

41

42 **Introduction**

43 In recent years advances in functional genomics has revolutionized our
44 understanding of the human genome. Evidence now points to the fact that
45 approximately 75% of the genome is transcribed but only ~1.2% of this is
46 responsible for encoding proteins (International Human Genome Sequencing
47 2004, Djebali et al. 2012). Of these recently identified elements, long non-
48 coding (lnc) RNAs are defined as transcripts exceeding 200 base pairs (bp) in
49 length with a lack of a functional open reading frame. Some lncRNAs are
50 dually classified as antisense (as) RNAs that are expressed from the same
51 locus as a sense transcript in the opposite orientation. Current estimates
52 using high-throughput transcriptome sequencing, indicate that up to 20-40%
53 of the approximately 20,000 protein-coding genes exhibit antisense
54 transcription (Chen et al. 2004, Katayama et al. 2005, Ozsolak et al. 2010).

55 The hypothesis that asRNAs play an important role in oncogenesis was first
56 proposed when studies increasingly found examples of aberrant expression of
57 these transcripts and other lncRNA subgroups in tumor samples (Balbin et al.
58 2015). Although studies characterizing the functional importance of asRNAs in
59 cancer are limited to date, characterization a number of individual transcripts
60 has led to the discovery of multiple examples of asRNA-mediated regulation
61 of several well-known tumorigenic factors (Yap et al. 2010, Johnsson et al.
62 2013). The mechanisms by which asRNAs accomplish this are diverse, and
63 include recruitment of chromatin modifying factors (Rinn et al. 2007), acting as

64 microRNA (miRNA) sponges (Memczak et al. 2013), and causing
65 transcriptional interference (Conley et al. 2012).

66

67 Responses to cellular stress, e.g. DNA damage, sustained oncogene
68 expression, and nutrient deprivation, are all tightly monitored and orchestrated
69 cellular pathways that are commonly dysregulated in cancer. Cellular
70 signaling in response to these types of cellular stress often converge on the
71 transcription factor TP53 that regulates transcription of coding and non-coding
72 downstream targets. One non-coding target of TP53 is the tumor suppressor
73 microRNA known as *miR34a* (Raver-Shapira et al. 2007).
74 Upon TP53 activation *miR34a* expression is increased allowing it to down-
75 regulate its targets involved in cellular pathways such as, growth factor
76 signaling, apoptosis, differentiation, and cellular senescence (Lal et al. 2011,
77 Slabakova et al. 2017). *miR34a* is a crucial factor in mediating activated TP53
78 response and it is often deleted or down-regulated in human cancers and has
79 been shown to be a valuable prognostic marker (Cole et al. 2008, Gallardo et
80 al. 2009, Zenz et al. 2009, Cheng et al. 2010, Liu et al. 2011).
81 Reduced *miR34a* transcription is mediated via epigenetic regulation in many
82 solid tumors, such as colorectal-, pancreatic-, and ovarian cancer (Vogt et al.
83 2011), as well as multiple types of hematological malignancies (Chim et al.
84 2010). In addition, *miR34a* has been shown to be transcriptionally regulated
85 via TP53 homologs, TP63 and TP73, other transcription factors, e.g. STAT3
86 and MYC, and, in addition, post-transcriptionally through miRNA sponging by
87 the NEAT1 lncRNA (Chang et al. 2008, Su et al. 2010, Agostini et al. 2011,
88 Rokavec et al. 2015, Ding et al. 2017). Despite these findings, the

89 mechanisms underlying *miR34a* regulation in the context of oncogenesis have
90 not yet been fully elucidated.

91

92 Studies across multiple cancer types have reported a decrease in oncogenic
93 phenotypes when *miR34a* expression is induced in a *TP53*-null background,
94 although endogenous mechanisms for achieving this have not yet been
95 discovered (Liu et al. 2011, Ahn et al. 2012, Yang et al. 2012, Stahlhut et al.
96 2015, Wang et al. 2015). In addition, previous reports from large-scale studies
97 interrogating global *TP53*-mediated regulation of lncRNAs have identified a
98 lncRNA originating in the antisense orientation from the *miR34a* locus which
99 is induced upon multiple forms of cellular stress (Rashi-Elkeles et al. 2014,
100 Hunten et al. 2015, Leveille et al. 2015, Ashouri et al. 2016, Kim et al.
101 2017). Despite this, none of these studies have continued to functionally
102 characterize this transcript. In this study, we functionally characterize
103 the *miR34a* asRNA transcript, and find that it positively regulates *miR34a*
104 expression resulting in a decrease of multiple tumorigenic phenotypes.
105 Furthermore, we find that *miR34a* asRNA-mediated up-regulation of *miR34a*
106 is sufficient to induce endogenous cellular mechanisms counteracting several
107 types of stress stimuli in a *TP53*-deficient background. Finally, similar to the
108 functional roles of antisense transcription at protein-coding genes, we identify
109 a rare example of an antisense RNA capable of regulating a cancer-
110 associated miRNA.

111

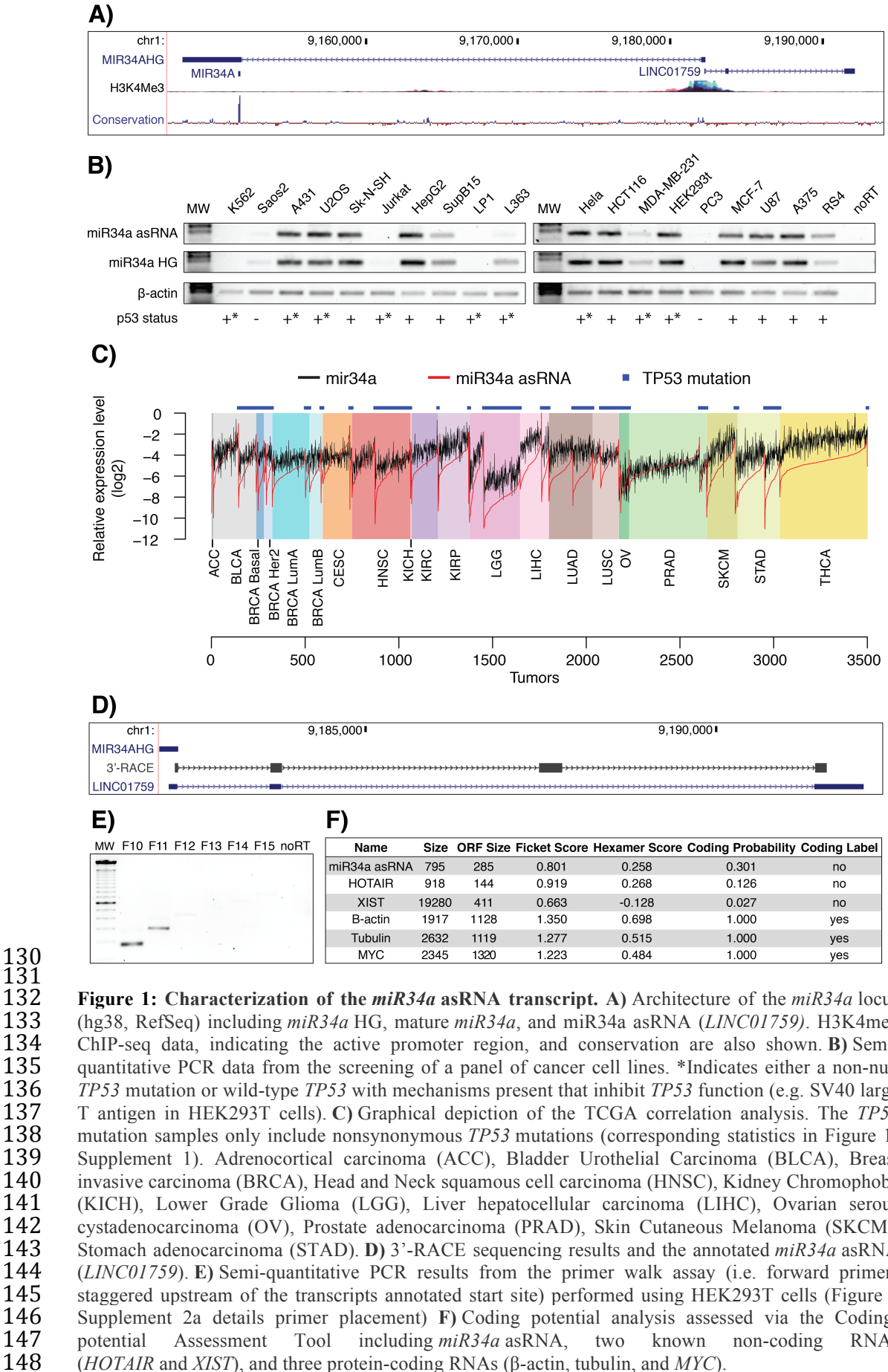
112 **Results**

113

114 ***miR34a* asRNA is a broadly expressed, non-coding transcript whose**
115 **levels correlate with *miR34a* expression**

116
117 miR34a asRNA is transcribed in a “head-to-head” orientation with
118 approximately 100 base pair overlap with the *miR34a* host gene (HG) (**Fig.**
119 **1a**). Due to the fact that sense/antisense pairs can be both concordantly and
120 discordantly expressed, we sought to evaluate this relationship in the case of
121 *miR34a* HG and its asRNA. Using a diverse panel of cancer cell lines, we
122 detected co-expression of both the *miR34a* HG and *miR34a* asRNA (**Fig. 1b**).
123 We included *TP53*+/+, *TP53* mutated, and *TP53*-/- cell lines in the panel due
124 to previous reports that *miR34a* is a known downstream target of *TP53*.
125 These results indicate that *miR34a* HG and *miR34a* asRNA are co-expressed
126 and that their expression levels correlate with *TP53* status, with *TP53*-/- cell
127 lines tending to have decreased or undetectable expression of both
128 transcripts.

129



149 We next sought to interrogate primary cancer samples to examine if a
150 correlation between *miR34a* asRNA and *miR34a* expression levels could be
151 identified. For this task we utilized RNA sequencing data from The Cancer
152 Genome Atlas (TCGA) after stratifying patients by cancer type, *TP53* status
153 and, where appropriate, cancer subtypes. The results indicate
154 that *miR34a* asRNA and *miR34a* expression are strongly correlated in the
155 vast majority of cancer types examined, both in the presence and absence of
156 wild-type *TP53* (**Fig. 1c, Figure 1-Figure Supplement 1a**). The results also
157 further confirm that the expression levels of both *miR34a* and its asRNA tend
158 to be reduced in patients with nonsynonymous *TP53* mutations (**Figure 1-**
159 **Figure Supplement 1b**).

160

161 Next, we aimed to gain a thorough understanding of *miR34a* asRNA's
162 molecular characteristics and cellular localization. To experimentally
163 determine the 3' termination site for the *miR34a* asRNA transcript we
164 performed 3' rapid amplification of cDNA ends (RACE) using the U2OS
165 osteosarcoma cell line that exhibited high endogenous levels
166 of *miR34a* asRNA in the cell panel screening. Sequencing the cloned cDNA
167 indicated that the transcripts 3' transcription termination site is 525 base pairs
168 upstream of the *LINC01759* transcript's annotated termination site (**Fig. 1d**).
169 Next, we characterized the *miR34a* asRNA 5' transcription start site by
170 carrying out a primer walk assay, i.e. a common reverse primer was placed in
171 exon 2 and forward primers were gradually staggered upstream of the
172 transcripts annotated start site (**Figure 1-Figure Supplement 2a**). Our results
173 indicated that the 5' start site for *miR34a* asRNA is in fact approximately 90bp

174 (F11 primer) to 220bp (F12 primer) upstream of the annotated start site (**Fig.**
175 **1e**). Polyadenylation status was evaluated via cDNA synthesis with either
176 random nanomers or oligoDT primers followed by semi-quantitative PCR with
177 results indicating that the *miR34a* asRNA is polyadenylated although the
178 unspliced form seems to only be in a polyadenylation negative state (**Figure**
179 **1-Figure Supplement 2b**). Furthermore, we investigated the propensity
180 of *miR34a* asRNA to be alternatively spliced in U2OS cells, using PCR
181 cloning and sequencing and found that the transcript is post-transcriptionally
182 spliced to form multiple different isoforms (**Figure 1-Figure Supplement 2c**).
183 Finally, to evaluate the subcellular localization of *miR34a* asRNA we utilized
184 RNA sequencing data from five cancer cell lines included in the ENCODE
185 (Consortium 2012) project that had been fractionated into cytosolic and
186 nuclear fractions. The analysis revealed that the *miR34a* asRNA transcript
187 localizes to both the nucleus and cytoplasm but primarily resides in the
188 nucleus (**Figure 1-Figure Supplement 2d**).

189
190 Finally, we utilized multiple approaches to evaluate the coding potential of
191 the *miR34a* asRNA transcript. The Coding-Potential Assessment Tool is a
192 bioinformatics-based tool that uses a logistic regression model to evaluate
193 coding-potential by examining ORF length, ORF coverage, Fickett score and
194 hexamer score (Wang et al. 2013). Results indicated that *miR34a* asRNA has
195 a similar lack of coding capacity to the known non-coding
196 transcripts *HOTAIR* and *XIST* and differs greatly when examining these
197 parameters to the known coding transcripts β -actin, tubulin, and *MYC* (**Fig.**
198 **1F**). We further confirmed these results using the Coding-Potential Calculator

199 that utilizes a support based machine-based classifier and accesses an
200 alternate set of discriminatory features (**Figure 1-Figure Supplement 2e**)
201 (Kong et al. 2007). *** We hope to be able to scan for peptides matching to
202 miR34a asRNA in CPTAC and Geiger et al., 2012 before submission and will
203 mention results here.***

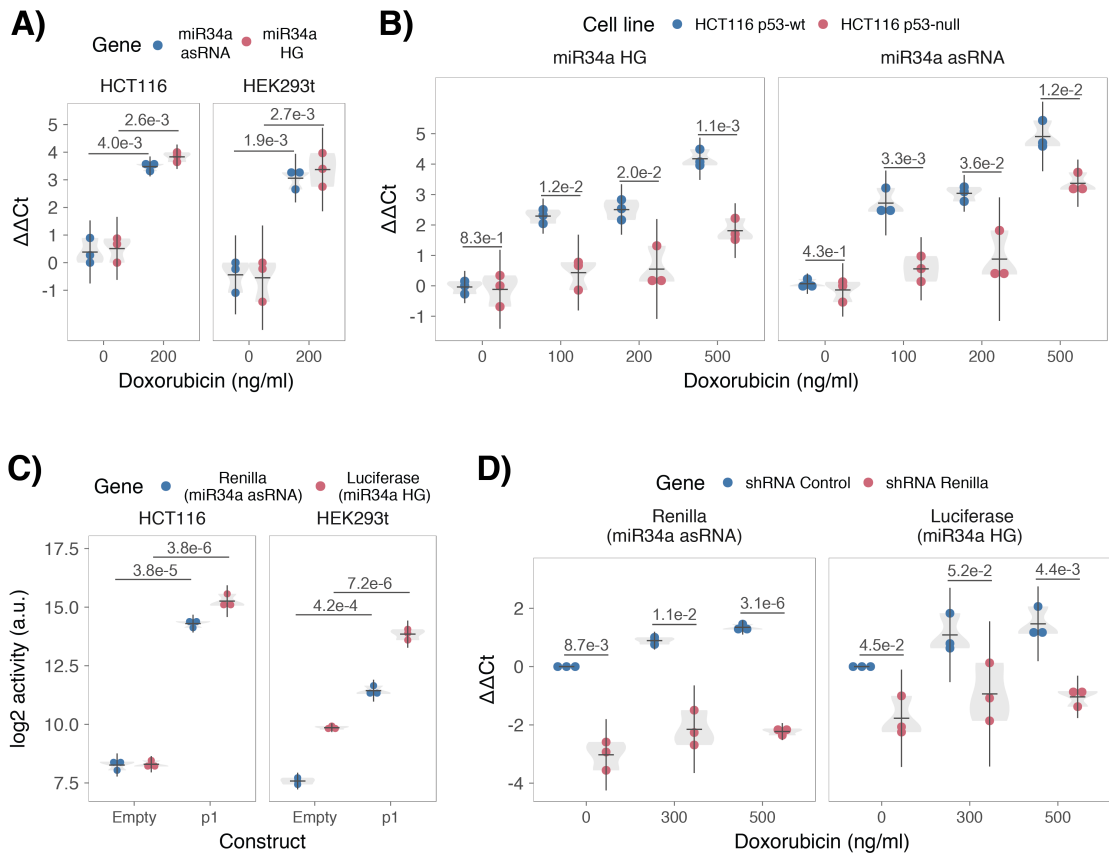
204

205 **TP53-mediated regulation of *miR34a* asRNA expression**

206 *miR34a* is a known downstream target of TP53 and has been previously
207 shown to exhibit increased expression within multiple contexts of cellular
208 stress. *miR34a* asRNA has also been shown to be induced upon TP53
209 activation in several global analyses of p53-regulated lncRNAs (Rashi-Elkeles
210 et al. 2014, Hunten et al. 2015, Leveille et al. 2015, Ashouri et al. 2016, Kim et
211 al. 2017). To confirm these results in our biological system, we treated
212 HEK293t, embryonic kidney cells, and HCT116, colorectal cancer cells, with
213 the DNA damaging agent doxorubicin to activate TP53. QPCR-mediated
214 measurement of both *miR34a* HG and asRNA indicated that their expression
215 levels were increased in response to doxorubicin treatment in both cell lines
216 (**Fig. 2a**). To assess if it is in fact TP53 that is responsible for the increase
217 in *miR34a* asRNA expression upon DNA damage, we
218 treated *TP53^{+/+}* and *TP53^{-/-}* HCT116 cells with increasing concentrations of
219 doxorubicin and monitored the expression of both *miR34a* HG and asRNA.
220 We observed a dose-dependent increase in both *miR34a* HG and asRNA
221 expression levels with increasing amounts of doxorubicin, indicating that
222 these two transcripts are co-regulated, although, this effect was largely
223 abrogated in *TP53^{-/-}* cells (**Fig. 2b**). These results indicate

224 that TP53 activation increases *miR34a* asRNA expression upon the induction
225 of DNA damage. Nevertheless, *TP53*^{-/-} cells also showed a dose-dependent
226 increase in both *miR34a* HG and asRNA, indicating that additional factors,
227 other than *TP53* are capable of initiating an increase in expression of both of
228 these transcripts upon DNA damage.

229



230

231 **Figure 2: TP53-mediated regulation of the *miR34a* locus.** **A)** Evaluating the effects of 24 hours of
 232 treatment with 200 ng/ml doxorubicin on *miR34a* asRNA and HG in HCT116 and HEK293t
 233 cells.* **B)** Monitoring *miR34a* HG and asRNA expression levels during 24 hours doxorubicin treatment
 234 in *TP53*^{+/+} and *TP53*^{-/-} HCT116 cells.* **C)** Quantification of luciferase and renilla levels after
 235 transfection of HCT116 and HEK293T cells with the p1 construct (Figure 2 Supplement 2 contains a
 236 schematic representation of the p1 construct).* **D)** HCT116 cells were co-transfected with the p1
 237 construct and shRNA renilla or shRNA control and subsequently treated with increasing doses of
 238 doxorubicin. 24 hours post-treatment, cells were harvested and renilla and luciferase levels were
 239 measured using QPCR. Resulting p-values from statistical testing are shown above the shRenilla
 240 samples which were compared to the shRNA control using the respective treatment condition.*
 241 *Individual points represent results from independent experiments and the gray shadow indicates the
 242 density of those points. Error bars show the 95% CI, black horizontal lines represent the mean, and p-
 243 values are shown over long horizontal lines indicating the comparison tested. All experiments in Figure
 244 2 were performed biological triplicate.
 245

246 The head-to head orientation of *miR34a* HG and asRNA, suggests that
247 transcription is initiated from a single promoter in a bi-directional manner (**Fig**
248 **1a**). To investigate whether *miR34a* HG and asRNA are transcribed from the
249 same promoter as divergent transcripts, we cloned the previously reported
250 *miR34a* HG promoter, including the TP53 binding site, into a luciferase/renilla
251 dual reporter vector which we hereafter refer to as p1 (**Figure 2-Figure**
252 **Supplement 1a-b**) (Raver-Shapira et al. 2007). Upon transfection of p1 into
253 HCT116 and HEK293t cell lines we observed increases in both luciferase and
254 renilla indicating that *miR34a* HG and asRNA expression can be regulated by
255 a single promoter contained within the p1 construct (**Fig. 2c**).

256

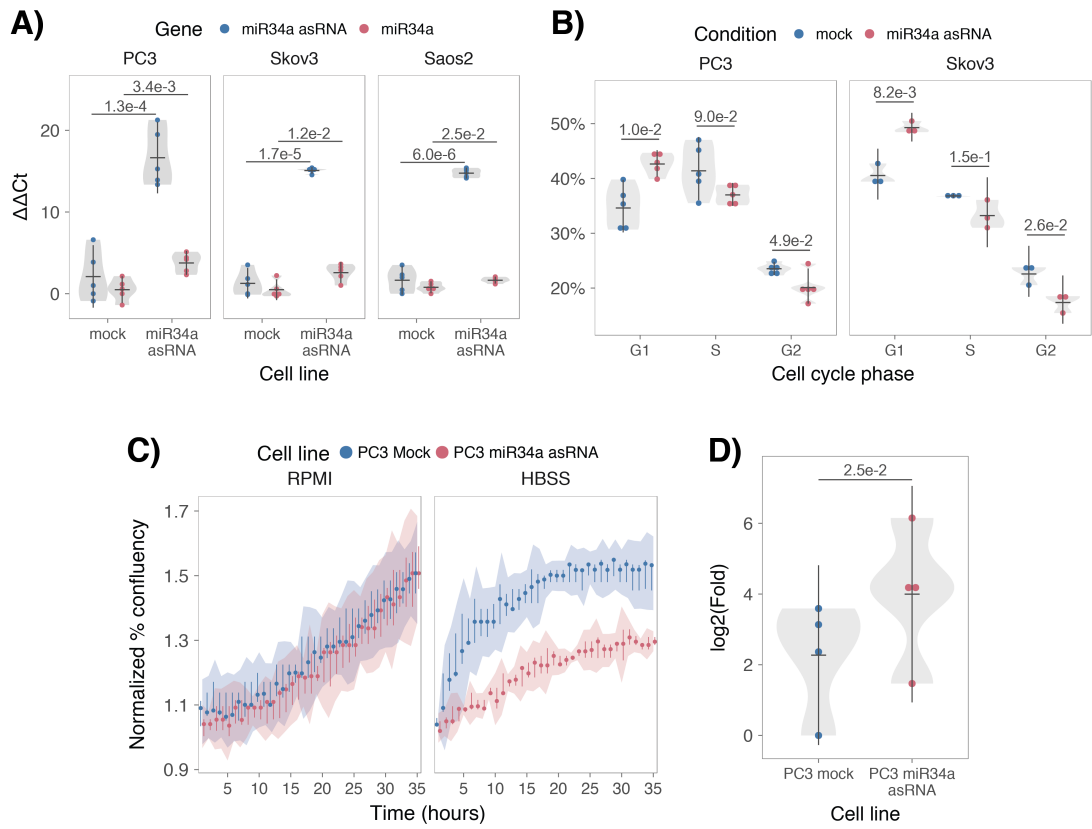
257 We hypothesized that *miR34a* asRNA may regulate *miR34a* HG levels and, in
258 addition, that the overlapping regions of the sense and antisense transcripts
259 may have a crucial role in mediating this regulation. Knockdown of
260 endogenous *miR34a* asRNA is complicated by its various isoforms (**Figure 1-**
261 **Figure Supplement 2c**). For this reason, we utilized the p1 construct to
262 evaluate the regulatory role of the *miR34a* asRNA on *miR34a* HG.
263 Accordingly, we first co-transfected the p1 construct, containing the
264 overlapping region of the two transcripts, and two different short hairpin (sh)
265 RNAs targeting renilla into HEK293T cells and subsequently measured
266 luciferase and renilla expression. The results indicated that shRNA-mediated
267 knock down of the p1-renilla transcript (corresponding to *miR34a* asRNA)
268 caused p1-luciferase (corresponding to *miR34a* HG) levels to concomitantly
269 decrease (**Figure 2-Figure Supplement 2**). These results indicate
270 that *miR34a* asRNA positively regulates levels of *miR34a* HG and that the

271 transcriptional product of the *miR34a* asRNA within in the p1 construct
272 contributes to inducing a miR34a response. To further support these
273 conclusions and better understand the role of *miR34a* asRNA during TP53
274 activation, *TP53^{+/+}* HCT116 cells were co-transfected with p1 and shRNA
275 renilla (2.1) and subsequently treated with increasing doses of doxorubicin.
276 Again, the results showed a concomitant reduction in luciferase levels upon
277 knock-down of p1-renilla i.e. the *miR34a* asRNA corresponding segment of
278 the p1 transcript (**Fig. 2d**). Furthermore, the results showed that in the
279 absence of p1-renilla the expected induction of p1-luciferase in response to
280 TP53 activation to DNA damage is abrogated. Collectively these results
281 indicate that *miR34a* asRNA positively regulates *miR34a* expression and is
282 crucial for an appropriate TP53-mediated *miR34a* response to DNA damage.

283

284 ***miR34a* asRNA regulates its host gene independently of TP53**
285 Despite the fact that TP53 regulates *miR34a* HG and asRNA expression, our
286 results indicated that other factors are also able to regulate this locus (**Fig.**
287 **2b**). Utilizing a lentiviral system, we stably over-expressed the *miR34a* asRNA
288 transcript in three *TP53*-null cell lines, PC3 (prostate cancer), Saos2
289 (osteogenic sarcoma), and Skov3 (ovarian adenocarcinoma). We first
290 analyzed the levels of *miR34a* asRNA in these stable over-expression cell
291 lines, compared to HEK293T cells, which have high endogenous levels
292 of *miR34a* asRNA. These results indicate that, on average, the over-
293 expression was approximately 30-fold higher in the over-expression cell lines
294 than in HEK293t cells. Due to the fact that *miR34a* asRNA can be up-
295 regulated ~30-fold in response to DNA damage (**Fig. 2b**), we deemed this

296 over-expression level to correspond to physiologically relevant levels in cells
297 encountering a stress stimulus, such as DNA damage (**Figure 3-Figure**
298 **Supplement 1**). Analysis of *miR34a* levels in the *miR34a* asRNA over-
299 expressing cell lines showed that this over-expression resulted in a
300 concomitant increase in the expression of *miR34a* in all three cell lines (**Fig.**
301 **3a**). These results indicate that, in the absence of *TP53*, *miR34a* expression
302 may be rescued by increasing the levels of *miR34a* asRNA expression.



303

304 **Figure 3: miR34a asRNA positively regulates miR34a and its associated phenotypes.** A) QPCR-
 305 mediated quantification of miR34a expression in cell lines stably over-
 306 expressing miR34a asRNA.* B) Cell cycle analysis comparing stably over-expressing miR34a asRNA
 307 cells to the respective mock expressing cells.* C) Analysis of cellular growth over time in miR34a
 308 asRNA over-expressing PC3 cells. Points represent the median from 3 independent experiments, the
 309 colored shadows indicate the 95% confidence interval, and vertical lines show the minimum and
 310 maximum values obtained from the three biological replicates. D) Differential phosphorylated
 311 polymerase II binding in miR34a asRNA over-expressing PC3 cells.* *Individual points represent
 312 results from independent experiments and the gray shadow indicates the density of those points. Error
 313 bars show the 95% CI, black horizontal lines represent the mean, and p-values are shown over long
 314 horizontal lines indicating the comparison tested.
 315

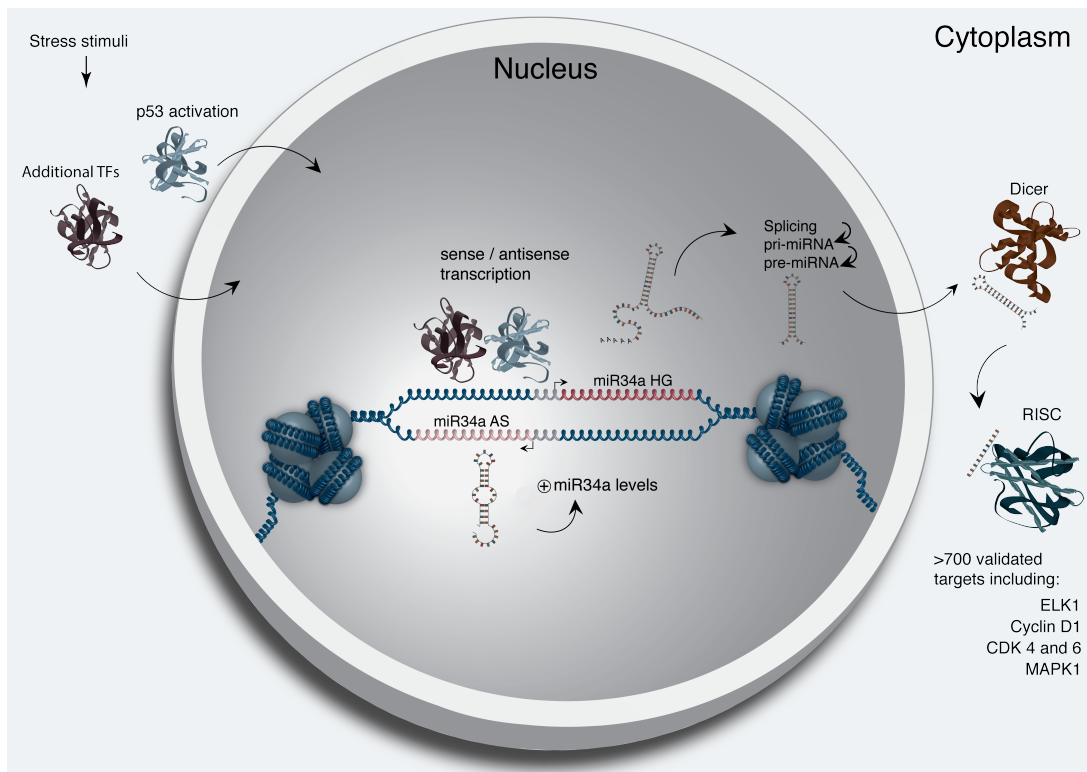
316 *miR34a* has been previously shown to regulate cell cycle progression, with
317 *miR34a* induction causing G1 arrest (Raver-Shapira et al. 2007, Tarasov et al.
318 2007). Cell cycle analysis via determination of DNA content showed a
319 significant increase in G1 phase cells in the PC3 and Skov3 *miR34a* asRNA
320 over-expressing cell lines, indicative of G1 arrest, as well as, a significant
321 decrease of cells in G2 phase (**Fig. 3b**). The effects of *miR34a* on the cell
322 cycle are mediated by its ability to target cell cycle regulators such as cyclin
323 D1 (*CCND1*) (Sun et al. 2008). We therefore sought to determine if
324 the *miR34a* asRNA over-expressing cell lines exhibited effects on this
325 known *miR34a* target. Quantification of both *CCND1* RNA expression (**Figure**
326 **3-Figure Supplement 2a**) and protein levels (**Figure 3-Figure Supplement**
327 **2b**) in the PC3 *miR34a* asRNA over-expressing cell line showed a significant
328 decrease of *CCND1* levels compared to the mock control. Collectively, these
329 results indicate that *miR34a* asRNA-mediated induction of *miR34a* is sufficient
330 to result in the corresponding *miR34a*-directed effects on cell cycle.

331
332 *miR34a* is also a well known inhibitor of cellular growth via its ability to
333 negatively regulate growth factor signaling. Furthermore, starvation has been
334 shown to induce *miR34a* expression that down-regulates multiple targets that
335 aid in the phosphorylation of pro-survival growth factors (Lal et al. 2011). We
336 further interrogated the effects of *miR34a* asRNA over-expression by
337 monitoring the growth of the cells in both normal and starvation conditions via
338 confluency measurements over a 35-hour period. Under normal growth
339 conditions there is a small but significant reduction ($p = 3.0\text{e-}8$) in confluency
340 in the *miR34a* asRNA over-expressing cell lines although, these effects on

341 cell growth are drastically increased in starvation conditions ($p = 9.5\text{e-}67$) (**Fig**
342 **3c**). This is in accordance with our previous results, and suggests
343 that *miR34a* asRNA-mediated increases in *miR34a* expression are crucial
344 under conditions of stress and necessary for the initiation of an appropriate
345 cellular response. In summary, we find that over-expression
346 of *miR34a* asRNA is sufficient to increase *miR34a* expression and gives rise
347 to known phenotypes observed with induction of *miR34a*.

348

349 Antisense RNAs have been reported to mediate their effects both via
350 transcriptional and post-transcriptional mechanisms. Due to the fact that
351 *miR34a* expression is undetected in wild type PC3 cells but, upon over-
352 expression of *miR34a* asRNA, increases to detectable levels, we
353 hypothesized that *miR34a* asRNA is capable of regulating *miR34a* expression
354 via a transcriptional mechanism. To ascertain if this is actually the case, we
355 performed chromatin immunoprecipitation (ChIP) for phosphorylated
356 polymerase II (polII) at the *miR34a* HG promoter in both *miR34a* asRNA over-
357 expressing and mock control cell lines. Our results indicated a clear increase
358 in phosphorylated polII binding at the *miR34a* promoter upon *miR34a* asRNA
359 over-expression indicating the ability of *miR34a* asRNA to regulate *miR34a*
360 levels on a transcriptional level (**Fig. 3d**).



361

362 **Figure 4: A graphical summary of the proposed *miR34a* asRNA function.** Stress stimuli,
 363 originating in the cytoplasm or nucleus, activates TP53 as well as additional factors. These factors then
 364 bind to the *miR34a* promoter and drive transcription of the sense and antisense strands. *miR34a* asRNA
 365 serves to increase the levels of *miR34a* HG transcription via an unknown mechanism. *miR34a* HG
 366 then, in turn, is then spliced, processed by the RNase III enzyme Drosha, and exported to the
 367 cytoplasm. The *miR34a* pre-miRNA then binds to Dicer where the hair-pin loop is cleaved and
 368 mature *miR34a* is formed. Binding of the mature *miR34a* miRNA to the RISC complex then allows it
 369 to bind and repress its targets.

370 **Discussion**

371
372 Multiple studies have previously shown asRNAs to be crucial for the
373 appropriate regulation of cancer-associated protein-coding genes and that
374 their dys-regulation can lead to a perturbation of tumor suppressive and
375 oncogenic pathways, as well as, cancer-related phenotypes (Yu et al. 2008,
376 Yap et al. 2010, Serviss et al. 2014, Balbin et al. 2015). Here we show that
377 asRNAs are also capable of regulating cancer-associated miRNAs resulting in
378 similar consequences as protein-coding gene dys-regulation (**Fig. 4**).
379 Interestingly, we show that, both in the presence and absence of
380 *TP53*, *miR34a* asRNA provides an additional regulatory level and functions by
381 mediating the increase of *miR34a* expression in both homeostasis and upon
382 encountering multiple forms of cellular stress. Furthermore, we find that
383 *miR34a* asRNA-mediated increases in *miR34a* expression levels are sufficient
384 to drive the appropriate cellular responses to multiple forms of stress stimuli
385 that are encountered (**Fig. 2d and Fig. 3c**). Previous studies have utilized
386 various molecular methods to up-regulate *miR34a* expression in a *TP53*-
387 deficient background showing similar phenotypic outcomes but, to our
388 knowledge, this is the first example of an endogenous mechanism by which
389 this can be achieved (Liu et al. 2011, Ahn et al. 2012, Yang et al. 2012,
390 Stahlhut et al. 2015, Wang et al. 2015).

391

392 In agreement with previous studies, we demonstrate that upon encountering
393 various types of cellular stress, *TP53* in concert with additional factors bind
394 and initiate transcription at the *miR34a* locus, thus increasing the levels of
395 *miR34a* asRNA and, in addition, *miR34a*. We hypothesize that *miR34a*

396 asRNA may provide positive feedback for *miR34a* expression whereby
397 *miR34a* asRNA serves as a scaffold for the recruitment of additional factors
398 that facilitate polymerase II-mediated transcription. In this manner, *miR34a*
399 expression is induced and thus, drives a shift towards a reduction in growth
400 factor signaling, senescence, and eventually apoptosis. On the other hand, in
401 cells without functional TP53, other factors, which typically act independently
402 or in concert with TP53, may initiate transcription of the *miR34a* locus. We
403 believe that *miR34a* asRNA could potentially be interacting directly with one of
404 these additional factors and recruiting it to the *miR34a* locus in order to drive
405 *miR34a* transcription. This is especially plausible due to head-to-head
406 orientation of the *miR34a* HG and asRNA, causing sequence complementarity
407 between the RNA and the promoter DNA. Previous reports have also
408 illustrated the ability of asRNAs to form hybrid DNA:RNA R-loops and, thus,
409 facilitate an open chromatin structure and the transcription of the sense gene
410 (Boque-Sastre et al. 2015). The fact that the p1 construct only contains a
411 small portion of the *miR34a* asRNA transcript indicates that this portion is
412 sufficient to give rise to at least a partial *miR34a* inducing response and
413 therefore, indicates that *miR34a* asRNA may be able to facilitate *miR34a*
414 expression independent of additional factors (**Fig 2d, Figure 2-Figure**
415 **Supplement 2a**). Nevertheless, further work will need to be performed to
416 ascertain the complete mechanism by which *miR34a* asRNA induces *miR34a*
417 expression.

418

419 An antisense transcript arising from the *miR34a* locus, *Lnc34a*, has been
420 previously reported to negatively regulate the expression of *miR34a* (Wang et

421 al. 2016). Although the *Lnc34a* and *miR34a* asRNA transcripts share some
422 sequence similarity, we believe them to be separate RNAs that are,
423 potentially, different isoforms of the same gene. We thoroughly address our
424 reasons for these beliefs and give appropriate supporting evidence in
425 (**Supplementary Document 1**). The fact that *Lnc34a* and *miR34a* asRNA
426 would appear to have opposing roles in their regulation of *miR34a* further
427 underlines the complexity of the regulation at this locus.

428

429 Clinical trials utilizing *miR34a* replacement therapy have previously been
430 conducted but, disappointingly, were terminated after adverse side effects of
431 an immunological nature were observed in several of the patients (Slabakova
432 et al. 2017). Although it is not presently clear if these side effects were caused
433 by *miR34a* or the liposomal carrier used to deliver the miRNA, the multitude of
434 evidence indicating *miR34a*'s crucial role in oncogenesis still makes its
435 therapeutic induction an interesting strategy for therapy and needs further
436 investigation. In summary, our results indicate that *miR34a* asRNA is a vital
437 player in the regulation of *miR34a* and is especially important in typical
438 examples of cellular stress encountered in cancer. We believe the
439 conclusions drawn in this study to be essential in the progress towards
440 developing a better understanding of the regulation of cancer-associated
441 miRNAs and, specifically, the tumor suppressor *miR34a*.

442

443 **Materials and Methods**

444 **Cell Culture**

445 All cell lines were cultured at 5% CO₂ and 37°C with HEK293T, Saos2, and

446 Skov3 cells cultured in DMEM high glucose (GE Healthcare Life Sciences,
447 Hyclone, Amersham. UK, Cat# SH30081), HCT116 and U2OS cells in
448 McCoy's 5a (ThermoFisher Scientific, Pittsburgh, MA, USA. Cat# SH30200),
449 and PC3 cells in RPMI (GE Healthcare Life Sciences, Hyclone, Cat#
450 SH3009602) and 2 mM L-glutamine (GE Healthcare Life Sciences, Hyclone,
451 Cat# SH3003402). All growth mediums were supplemented with 10% heat-
452 inactivated FBS (ThermoFisher Scientific, Gibco, Cat# 12657029) and 50
453 µg/ml of streptomycin (ThermoFisher Scientific, Gibco, Cat# 15140122) and
454 50 µg/ml of penicillin (ThermoFisher Scientific, Gibco, Cat# 15140122). All cell
455 lines were purchased from ATCC, tested negative for mycoplasma, and their
456 identity was verified via STR profiling.

457

458 **Bioinformatics, Data Availability, and Statistical Testing**

459 The USCS genome browser (Kent et al. 2002) was utilized for the
460 bioinformatic evaluation of antisense transcription utilizing the RefSeq
461 (O'Leary et al. 2016) gene annotation track.

462

463 All raw experimental data, code used for analysis, and supplementary
464 methods are available for review at ([Serviss 2017](#)) and are provided as an R
465 package. All analysis took place using the R statistical programming language
466 (Team 2017) using multiple external packages that are all documented in the
467 package associated with this article (Wilkins , Chang 2014, Wickham 2014,
468 Wickham 2016, Allaire et al. 2017, Arnold 2017, Wickham 2017, Wickham
469 2017, Wickham 2017, Xiao 2017, Xie 2017). The package facilitates
470 replication of the operating system and package versions used for the original
471 analysis, reproduction of each individual figure and figure supplement

472 included in the article, and easy review of the code used for all steps of the
473 analysis, from raw-data to figure.

474

475 The significance threshold (alpha) in this study was set to 0.05. Statistical
476 testing was performed using a unpaired two sample Student's t-test unless
477 otherwise specified.

478

479 **Coding Potential**

480 Protein-coding capacity was evaluated using the Coding-potential
481 Assessment Tool (Wang et al. 2013) and Coding-potential Calculator (Kong et
482 al. 2007) with default settings. Transcript sequences for use with Coding-
483 potential Assessment Tool were downloaded from the UCSC genome
484 browser using the Ensembl
485 accessions: *HOTAIR* (ENST00000455246), *XIST* (ENST00000429829), β-
486 actin (ENST00000331789), Tubulin (ENST00000427480),
487 and *MYC* (ENST00000377970). Transcript sequences for use with Coding-
488 potential Calculator were downloaded from the UCSC genome browser using
489 the following IDs: *HOTAIR* (uc031qho.1), β-actin (uc003soq.4).

490

491 **shRNAs**

492 shRNA-expressing constructs were cloned into the U6M2 construct using the
493 BgIII and KpnI restriction sites as previously described (Amarzguioui et al.
494 2005). shRNA constructs were transfected using Lipofectamine 2000 or 3000
495 (ThermoFisher Scientific, Cat# 12566014 and L3000015). The sequences
496 targeting renilla is as follows: shRenilla 1.1 (AAT ACA CCG CGC TAC TGG

497 C), shRenilla 2.1 (TAA CGG GAT TTC ACG AGG C).

498

499 **Bi-directional Promoter Cloning**

500 The overlapping region (p1) corresponds with the sequence previously
501 published as the TP53 binding site in (Raver-Shapira et al. 2007) which we
502 synthesized, cloned into the pLucRluc construct (Polson et al. 2011) and
503 sequenced to verify its identity.

504

505 **Promoter Activity**

506 Cells were co-transfected with the renilla/firefly bidirectional promoter
507 construct (Polson et al. 2011) and GFP by using Lipofectamine 2000 (Life
508 Technologies, Cat# 12566014). The expression of GFP and luminescence
509 was measured 24 h post transfection by using the Dual-Glo Luciferase Assay
510 System (Promega, Cat# E2920) and detected by the GloMax-Multi+ Detection
511 System (Promega, Cat# SA3030). The expression of luminescence was
512 normalized to GFP.

513

514 **Generation of U6-expressed miR34a AS Lentiviral Constructs**

515 The U6 promoter was amplified from the U6M2 cloning plasmid (Amarzguioui
516 et al. 2005) and ligated into the Not1 restriction site of the pHIV7-IMPDH2
517 vector (Turner et al. 2012). *miR43a* asRNA was PCR amplified and
518 subsequently cloned into the Nhe1 and Pac1 restriction sites in the pHIV7-
519 IMPDH2-U6 plasmid.

520

521 **Lentiviral Particle production, infection, and selection**

522 Lentivirus production was performed as previously described in (Turner et al.
523 2012). Briefly, HEK293T cells were transfected with viral and expression
524 constructs using Lipofectamine 2000 (ThermoFisher Scientific, Cat#
525 12566014), after which viral supernatants were harvested 48 and 72 hours
526 post-transfection. Viral particles were concentrated using PEG-IT solution
527 (Systems Biosciences, Palo Alto, CA, USA. Cat# LV825A-1) according to the
528 manufacturer's recommendations. HEK293T cells were used for virus titration
529 and GFP expression was evaluated 72hrs post-infection via flow cytometry
530 (LSRII, BD Biosciences, San Jose, CA, USA) after which TU/ml was
531 calculated.

532

533 Stable lines were generated by infecting cells with a multiplicity of infection of
534 1 after which 1-2 µM mycophenolic acid (Merck, Kenilworth, NJ, USA. Cat#
535 M5255) selection was initiated 48 hours post-infection. Cells were expanded
536 as the selection process was monitored via flow cytometry analysis (LSRII,
537 BD Biosciences) of GFP and selection was terminated once > 90% of the
538 cells were GFP positive. Quantification of *miR34a* asRNA over-expression
539 and *miR34a* was performed in biological quintuplet for all cell lines.

540

541 **Western Blotting**

542 Samples were lysed in 50 mM Tris-HCl (Sigma Aldrich, St. Louis, MO, USA.
543 Cat# T2663), pH 7.4, 1% NP-40 (Sigma Aldrich, Cat# I8896), 150 mM NaCl
544 (Sigma Aldrich, Cat# S5886), 1 mM EDTA (Promega, Madison, WI, USA.
545 Cat# V4231), 1% glycerol (Sigma Aldrich, Cat# G5516), 100 µM vanadate
546 (Sigma Aldrich, Cat# S6508), protease inhibitor cocktail (Roche Diagnostics,

547 Basel, Switzerland, Cat# 004693159001) and PhosSTOP (Roche
548 Diagnostics, Cat# 04906837001). Lysates were subjected to SDS-PAGE and
549 transferred to PVDF membranes. The proteins were detected by western blot
550 analysis by using an enhanced chemiluminescence system (Western
551 Lightning-ECL, PerkinElmer, Waltham, MA, USA. Cat# NEL103001EA).
552 Antibodies used were specific for CCND1 1:1000 (Cell Signaling, Danvers,
553 MA, USA. Cat# 2926), and β-actin 1:5000 (Sigma-Aldrich, Cat# A5441). All
554 western blot quantifications were performed using ImageJ (Schneider et al.
555 2012).

556

557 **RNA Extraction and cDNA Synthesis**

558 For downstream SYBR green applications, RNA was extracted using the
559 RNeasy mini kit (Qiagen, Venlo, Netherlands, Cat# 74106) and subsequently
560 treated with DNase (Ambion Turbo DNA-free, ThermoFisher Scientific, Cat#
561 AM1907). 500ng RNA was used for cDNA synthesis using MuMLV
562 (ThermoFisher Scientific, Cat# 28025013) and a 1:1 mix of oligo(dT) and
563 random nanomers.

564

565 For analysis of miRNA expression with Taqman, samples were isolated with
566 TRIzol reagent (ThermoFisher Scientific, Cat# 15596018) and further
567 processed with the miRNeasy kit (Qiagen, Cat# 74106). cDNA synthesis was
568 performed using the TaqMan MicroRNA Reverse Transcription Kit
569 (ThermoFisher Scientific, Cat# 4366597) using the corresponding oligos
570 according to the manufacturer's recommendations.

571

572 **QPCR and PCR**

573 PCR was performed using the KAPA2G Fast HotStart ReadyMix PCR Kit
574 (Kapa Biosystems, Wilmington, MA, USA, Cat# KK5601) with corresponding
575 primers. QPCR was carried out using KAPA 2G SYBRGreen (Kapa
576 Biosystems, Cat# KK4602) using the Applied Biosystems 7900HT machine
577 with the cycling conditions: 95 °C for 3 min, 95 °C for 3 s, 60 °C for 30 s.

578

579 QPCR for miRNA expression analysis was performed according to the primer
580 probe set manufacturers recommendations (ThermoFisher Scientific) and
581 using the TaqMan Universal PCR Master Mix (ThermoFisher Scientific, Cat#
582 4304437) with the same cycling scheme as above. Primer and probe sets for
583 TaqMan were also purchased from ThermoFisher Scientific (Life
584 Technologies at time of purchase, TaqMan® MicroRNA Assay, hsa-miR-34a,
585 human, Cat# 4440887, Assay ID: 000426 and Control miRNA Assay, RNU48,
586 human, Cat# 4440887, Assay ID: 001006).

587

588 The $\Delta\Delta Ct$ method was used to quantify gene expression. All QPCR-based
589 experiments were performed in at least technical duplicate. Primers for all
590 PCR-based experiments are listed in **Supplementary Document 2** and
591 arranged by figure.

592

593 **Cell Cycle Distribution**

594 Cells were washed in PBS and fixed in 4% paraformaldehyde at room
595 temperature overnight. Paraformaldehyde was removed, and cells were re-
596 suspended in 95% EtOH. The samples were then rehydrated in distilled

597 water, stained with DAPI and analyzed by flow cytometry on a LSRII (BD
598 Biosciences) machine. Resulting cell cycle phases were quantified using the
599 ModFit software (Verity Software House, Topsham, ME, USA). Experiments
600 were performed in biological quadruplet (PC3) or triplicate (Skov3). The log2
601 fraction of cell cycle phase was calculated for each replicate a two sample t-
602 test was utilized for statistical testing.

603

604 **3' Rapid Amplification of cDNA Ends**

605 3'-RACE was performed as described as previously in (Johnsson et al. 2013).
606 Briefly, U2OS cell RNA was polyA-tailed using yeast polyA polymerase
607 (ThermoFisher Scientific, Cat# 74225Z25KU) after which cDNA was
608 synthesized using oligo(dT) primers. Nested-PCR was performed first using a
609 forward primer in *miR34a* asRNA exon 1 and a tailed oligo(dT) primer
610 followed by a second PCR using an alternate *miR34a* asRNA exon 1 primer
611 and a reverse primer binding to the tail of the previously used oligo(dT)
612 primer. PCR products were gel purified and cloned the Strata Clone Kit
613 (Agilent Technologies, Santa Clara, CA, USA. Cat# 240205), and sequenced.

614

615 **Chromatin Immunoprecipitation**

616 The ChIP was performed as previously described in (Johnsson et al. 2013)
617 with the following modifications. Cells were crosslinked in 1% formaldehyde
618 (Merck, Cat# 1040039025), quenched with 0.125M glycine (Sigma Aldrich,
619 Cat# G7126), and lysed in cell lysis buffer comprised of: 5mM PIPES (Sigma
620 Aldrich, Cat# 80635), 85mM KCL (Merck, Cat# 4936), 0.5% NP40 (Sigma
621 Aldrich, Cat# I8896), protease inhibitor (Roche Diagnostics, Cat#

622 004693159001). Samples were then sonicated in 50mM TRIS-HCL pH 8.0
623 (Sigma Aldrich, MO, USA, Cat# T2663) 10mM EDTA (Promega, WI, USA,
624 Cat# V4231), 1% SDS (ThermoFisher Scientific, Cat# AM9822), and protease
625 inhibitor (Roche Diagnostics, Cat# 004693159001) using a Bioruptor
626 Sonicator (Diagenode, Denville, NJ, USA). Samples were incubated over
627 night at 4°C with the polII antibody (Abcam, Cambridge, UK, Cat# ab5095)
628 and subsequently pulled down with Salmon Sperm DNA/Protein A Agarose
629 (Millipore, Cat# 16-157) beads. DNA was eluted in an elution buffer of 1%
630 SDS (ThermoFisher Scientific, Cat# AM9822) 100mM NaHCO3 (Sigma
631 Aldrich, Cat# 71631), followed by reverse crosslinking, RNaseA
632 (ThermoFisher Scientific, Cat# 1692412) and protease K (New England
633 Biolabs, Ipswich, MA, USA, Cat# P8107S) treatment. The DNA was eluted
634 using Qiagen PCR purification kit (Cat# 28106) and quantified via QPCR.
635 QPCR was performed in technical duplicate using the standard curve method
636 and reported absolute values. The fraction of input was subsequently
637 calculated using the mean of the technical replicates followed by calculating
638 the fold over the control condition. Statistical testing was performed using 4
639 biological replicates with the null hypothesis that the true log 2 fold change
640 values were equal to zero.

641

642 **Confluency Analysis**

643 Cells were incubated in the Spark Multimode Microplate (Tecan, Männedorf,
644 Switzerland) reader for 48 hours at 37°C with 5% CO₂ in a humidity chamber.
645 Confluency was measured every hour using bright-field microscopy and the
646 percentage of confluency was reported via the plate reader's inbuilt algorithm.

647 Percentage of confluence was normalized to the control sample in each
648 condition (shown in figure) and then ranked to move the data to a linear scale.
649 Using the mean of the technical duplicates in three biological replicates, the
650 rank was then used to construct a linear model, of the dependency of the rank
651 on the time and cell lines variables for each growth condition. Reported p-
652 values are derived from the t-test, testing the null hypothesis that the
653 coefficient estimate of the cell line variable is equal to 0.

654

655 **Pharmacological Compounds**

656 Doxorubicin was purchased from Teva (Petah Tikva, Israel, cat. nr. 021361).

657

658 **Cellular Localization Analysis**

659 Quantified RNAseq data from 11 cell lines from the GRCh38 assembly was
660 downloaded from the ENCODE project database and quantifications for
661 *miR34a* asRNA (ENSG00000234546), GAPDH (ENSG00000111640), and
662 MALAT1 (ENSG00000251562) were extracted. Cell lines for which data was
663 downloaded include: A549, GM12878, HeLa-S3, HepG2, HT1080, K562
664 MCF-7, NCI-H460, SK-MEL-5, SK-N-DZ, SK-N-SH. Initial exploratory analysis
665 revealed that several cell lines should be removed from the analysis due to a)
666 a larger proportion of GAPDH in the nucleus than cytoplasm or b) variation of
667 *miR34a* asRNA expression is too large to draw conclusions, or c) they have
668 no or low (<6 TPM) *miR34a* asRNA expression. Furthermore, only
669 polyadenylated libraries were used in the final analysis, due to the fact that
670 the cellular compartment enrichment was improved in these samples. All
671 analyzed genes are reported to be polyadenylated. In addition, only samples

672 with 2 biological replicates were retained. For each cell type, gene, and
673 biological replicate the fraction of transcripts per million (TPM) in each cellular
674 compartment was calculated as the fraction of TPM in the specific
675 compartment by the total TPM. The mean and standard deviation for the
676 fraction was subsequently calculated for each cell type and cellular
677 compartment and this information was represented in the final figure.

678

679 **CAGE Analysis**

680 All available CAGE data from the ENCODE project (Consortium 2012) for 36
681 cell lines was downloaded from the UCSC genome browser (Kent et al. 2002)
682 for genome version hg19. Of these, 28 cell lines had CAGE transcription start
683 sites (TSS) mapping to the plus strand of chromosome 1 and in regions
684 corresponding to 200 base pairs upstream of the *lnc34a* start site (9241796 -
685 200) and 200 base pairs upstream of the GENCODE
686 annotated *miR34a* asRNA start site (9242263 + 200). These cell lines
687 included: HFDPC, H1-hESC, HMEpC, HAoEC, HPIEpC, HSaVEC, GM12878,
688 hMSC-BM, HUVEC, AG04450, hMSC-UC, IMR90, NHDF, SK-N-SH_RA, BJ,
689 HOB, HPC-PL, HAoAF, NHEK, HVMF, HWP, MCF-7, HepG2, hMSC-AT,
690 NHEM.f_M2, SkMC, NHEM_M2, and HCH. In total 74 samples were included.
691 17 samples were polyA-, 47 samples were polyA+, and 10 samples were total
692 RNA. In addition, 34 samples were whole cell, 15 enriched for the cytosolic
693 fraction, 15 enriched for the nucleolus, and 15 enriched for the nucleus. All
694 CAGE transcription start sites were plotted and the RPKM of the individual
695 reads was used to color each read to indicate their relative abundance. In
696 cases where CAGE TSS spanned identical regions, the RPMKs of the regions

697 were summed and represented as one CAGE TSS in the figure. In addition, a
698 density plot shows the distribution of the CAGE reads in the specified
699 interval.

700

701 **Splice Junction Analysis**

702 All available whole cell (i.e. non-fractionated) spliced read data originating
703 from the Cold Spring Harbor Lab in the ENCODE project (Consortium 2012)
704 for 38 cell lines was downloaded from the UCSC genome browser (Kent et al.
705 2002). Of these cell lines, 36 had spliced reads mapping to the plus strand of
706 chromosome 1 and in the region between the *lnc34a* start (9241796) and
707 transcription termination (9257102) site (note that *miR34a* asRNA resides
708 totally within this region). Splice junctions from the following cell lines were
709 included in the final figure: A549, Ag04450, Bj, CD20, CD34 mobilized,
710 Gm12878, H1hesc, Haoaf, Haoec, Hch, Helas3, Hepg2, Hfdpc, Hmec,
711 Hmepc, Hmescat, Hmscbm, Hmscuc, Hob, Hpcpl, Hpiepc, Hsavec, Hsmm,
712 Huvec, Hvmf, Hwp, Imr90, Mcf7, Monocd14, Nhdf, Nhek, Nhemfm2,
713 Nhemm2, Nhlf, Skmc, and Sknsh. All splice junctions were included in the
714 figure and colored according to the number of reads corresponding to each. In
715 cases where identical reads were detected multiple times, the read count was
716 summed and represented as one read in the figure.

717

718 **TCGA Expression and Correlation Analysis**

719 Erik/Jimmy should probably take this.

720

721 **Acknowledgments**

722 Henry (?), Mattias(?), Martin(?)

723

724 **Competing Interests**

725

726 The authors declare no competing interests.

727

728

729 **Funding**

730

731 This work has been supported by the Swedish Research Council [521-2012-
732 2037], Swedish Cancer Society [150768], Cancer Research Foundations of
733 Radiumhemmet [144063] and the Swedish Childhood Cancer Foundation
734 [PR2015-0009].

735

736

737 **Figure Supplements**

738

739 Figure 1-Supplement 1: TCAG expression levels and correlation analysis
740 statistics.

741

742 Figure 1-Supplement 2: Molecular characteristics of miR34a asRNA.

743

744 Figure 2-Supplement 1: A schematic representation of the p1 construct.

745

746 Figure 2-Supplement 2: Evaluating the effects of miR34a asRNA down-
747 regulation.

748

749 Figure 3-Supplement 1: Physiological relevance of miR34a asRNA
750 overexpression.

751

752 Figure 3-Supplement 2: Effects of miR34a asRNA overexpression on cyclin
753 D1.

754

755 Supplementary Document 1: Evaluating the relationship between miR34a
756 asRNA and lnc34a.

757

758 Supplementary Document 2: A table of primers used in this study.

759 **Supplementary Figures**

760

A)

| cancer | all n | all rho | all p | TP53wt n | TP53wt rho | TP53wt p | TP53mut n | TP53mut rho | TP53mut p |
|------------|-------|----------|----------|----------|------------|----------|-----------|-------------|-----------|
| ACC | 10 | 5.52e-01 | 1.04e-01 | 10 | 5.52e-01 | 1.04e-01 | NA | NA | NA |
| BLCA | 228 | 5.15e-01 | 7.89e-17 | 134 | 4.53e-01 | 3.86e-08 | 94 | 4.27e-01 | 1.73e-05 |
| BRCA Basal | 42 | 5.74e-01 | 9.54e-05 | 10 | 6.24e-01 | 6.02e-02 | 32 | 5.74e-01 | 7.41e-04 |
| BRCA Her2 | 44 | 1.47e-01 | 3.39e-01 | 12 | 2.24e-01 | 4.85e-01 | 32 | 6.82e-02 | 7.10e-01 |
| BRCA LumA | 199 | 3.41e-01 | 8.22e-07 | 177 | 3.43e-01 | 2.96e-06 | 22 | 4.86e-01 | 2.31e-02 |
| BRCA LumB | 70 | 1.71e-01 | 1.57e-01 | 61 | 1.48e-01 | 2.53e-01 | 9 | 1.67e-01 | 6.78e-01 |
| CESC | 156 | 1.39e-01 | 8.37e-02 | 145 | 1.60e-01 | 5.45e-02 | 11 | -4.55e-02 | 9.03e-01 |
| HNSC | 313 | 5.37e-01 | 8.38e-25 | 123 | 6.08e-01 | 0.00e+00 | 190 | 4.47e-01 | 9.68e-11 |
| KICH | 5 | 6.00e-01 | 3.50e-01 | 5 | 6.00e-01 | 3.50e-01 | NA | NA | NA |
| KIRC | 142 | 3.49e-01 | 2.06e-05 | 141 | 3.37e-01 | 4.41e-05 | NA | NA | NA |
| KIRP | 167 | 4.51e-01 | 9.16e-10 | 163 | 4.48e-01 | 2.04e-09 | 4 | 8.00e-01 | 3.33e-01 |
| LGG | 271 | 6.33e-01 | 9.92e-32 | 76 | 7.28e-01 | 0.00e+00 | 195 | 3.87e-01 | 2.26e-08 |
| LIHC | 153 | 5.63e-01 | 3.64e-14 | 114 | 5.16e-01 | 4.18e-09 | 39 | 4.55e-01 | 3.95e-03 |
| LUAD | 234 | 2.82e-01 | 1.15e-05 | 128 | 3.61e-01 | 2.87e-05 | 106 | 2.27e-01 | 1.91e-02 |
| LUSC | 139 | 2.29e-01 | 6.74e-03 | 42 | 4.17e-02 | 7.93e-01 | 97 | 3.29e-01 | 9.91e-04 |
| OV | 56 | 2.33e-01 | 8.37e-02 | 10 | 8.42e-01 | 4.46e-03 | 46 | 1.46e-01 | 3.31e-01 |
| PRAD | 413 | 4.66e-01 | 1.33e-23 | 375 | 4.59e-01 | 6.13e-21 | 38 | 4.50e-01 | 4.58e-03 |
| SKCM | 165 | 6.48e-01 | 5.43e-21 | 152 | 6.10e-01 | 7.85e-17 | 13 | 4.34e-01 | 1.40e-01 |
| STAD | 225 | 3.72e-01 | 8.23e-09 | 145 | 3.67e-01 | 5.71e-06 | 80 | 4.20e-01 | 1.03e-04 |
| THCA | 469 | 4.58e-01 | 1.07e-25 | 467 | 4.62e-01 | 4.06e-26 | NA | NA | NA |

B)

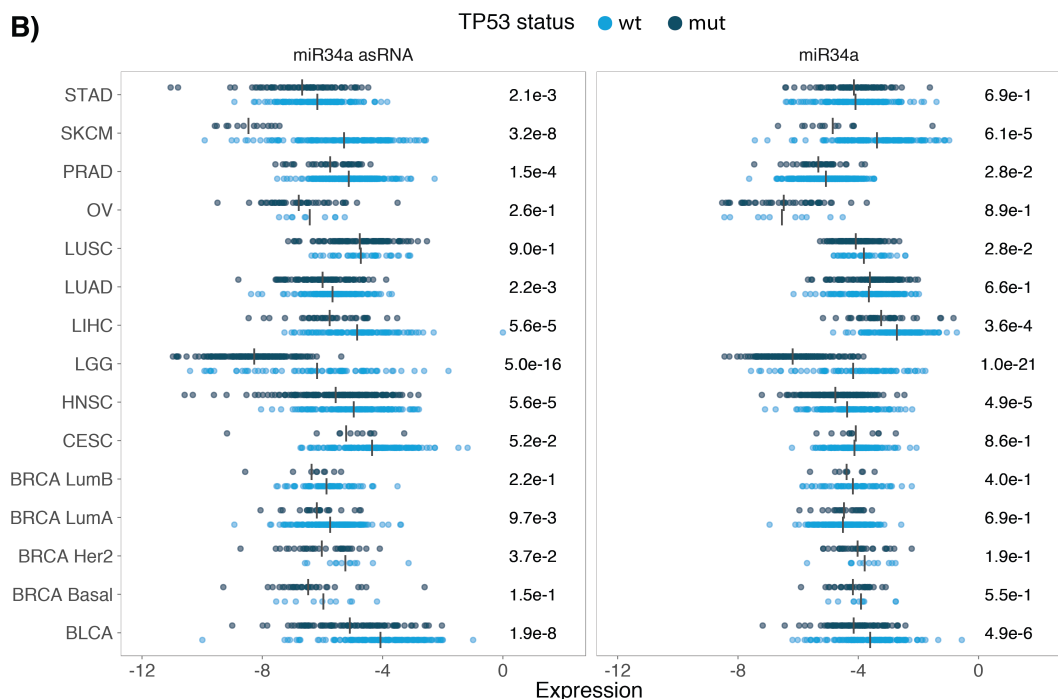
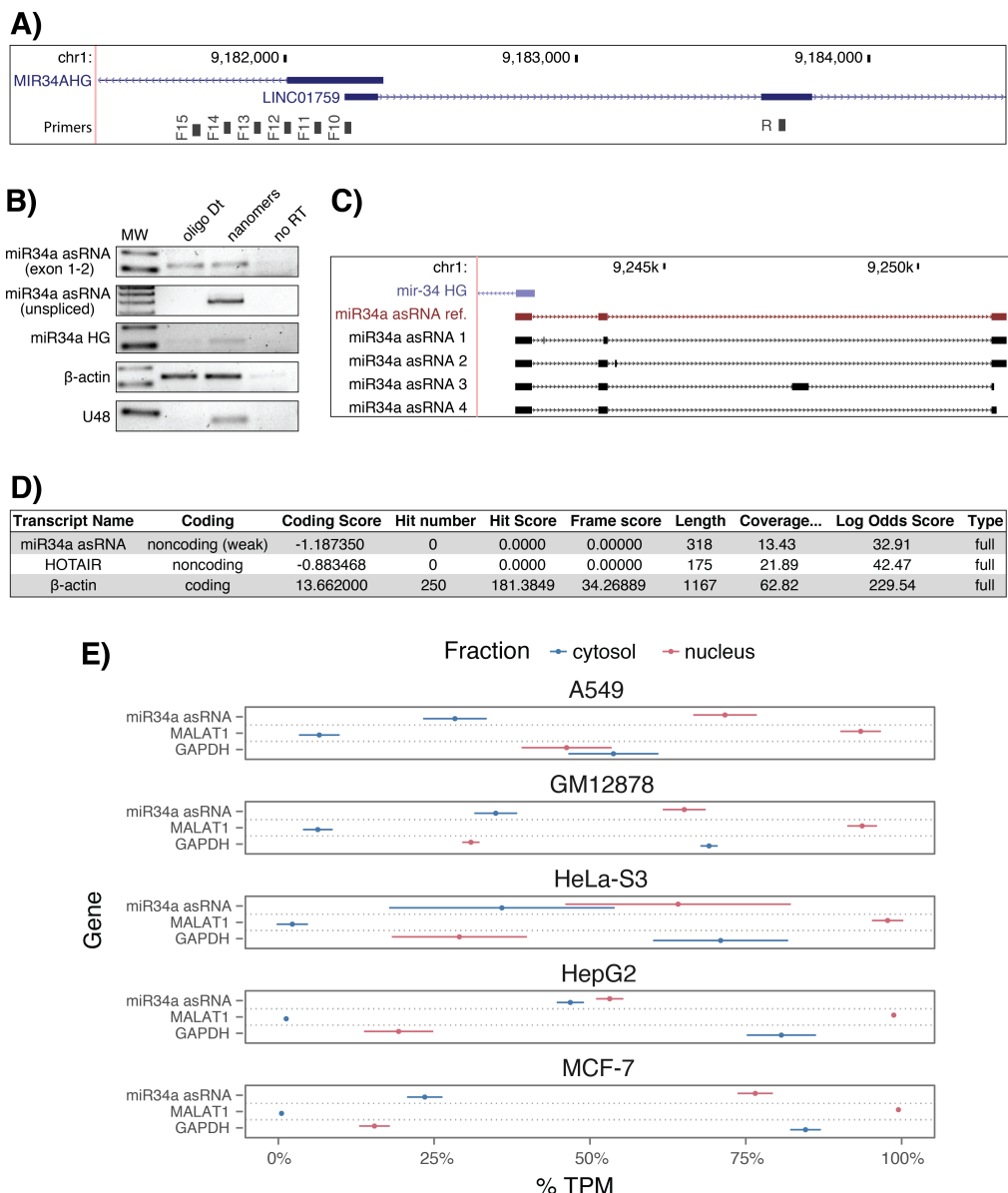


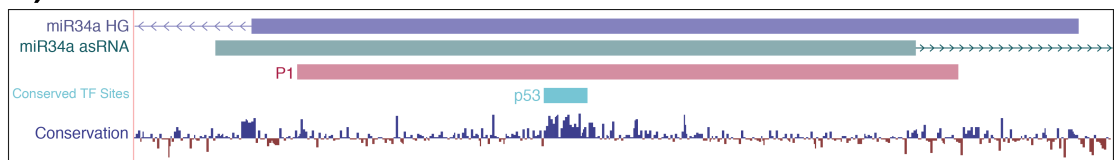
Figure 1 Supplement 1: TCAG expression levels and correlation analysis statistics. A) Spearman's rho and p-values (p) from the correlation analysis in Figure 1a. B) Expression levels of *miR34a* and *miR34a* asRNA in *TP53* wt and nonsynonymous mutation samples. P-values are indicated on the right side of each panel are derived from comparing the *TP53* wild type samples to the samples with a nonsynonymous mutation. Vertical lines indicate the mean. Bladder Urothelial Carcinoma (BLCA), Breast invasive carcinoma (BRCA), Head and Neck squamous cell carcinoma (HNSC), Lower Grade Glioma (LGG), Liver hepatocellular carcinoma (LIHC), Lung adenocarcinoma (LUAD), Lung squamous cell carcinoma (LUSC), Ovarian serous cystadenocarcinoma (OV), Prostate adenocarcinoma (PRAD), Skin Cutaneous Melanoma (SKCM), Stomach adenocarcinoma (STAD).



772
773

774 **Figure 1 Supplement 2: Molecular characteristics of *miR34a* asRNA.** A) A schematic
775 representation of the primer placement in the primer walk assay. B) Polyadenylation status of spliced
776 and unspliced *miR34a* asRNA in HEK293T cells. C) Sequencing results from the analysis
777 of *miR34a* asRNA isoforms in U2OS cells. *miR34a* AS ref. refers to the full-length transcript as
778 defined by the 3'-RACE and primer walk assay. D) Analysis of coding potential of the *miR34a* asRNA
779 transcript using the Coding-potential Calculator. E) RNAseq data from five fractionated cell lines in
780 the ENCODE project showing the percentage of transcripts per million (TPM) for *miR34a* asRNA.
781 MALAT1 (nuclear localization) and GAPDH (cytoplasmic localization) are included as fractionation
782 controls. Points represent the mean and horizontal lines represent the standard deviation from two
783 biological replicates.
784

A)

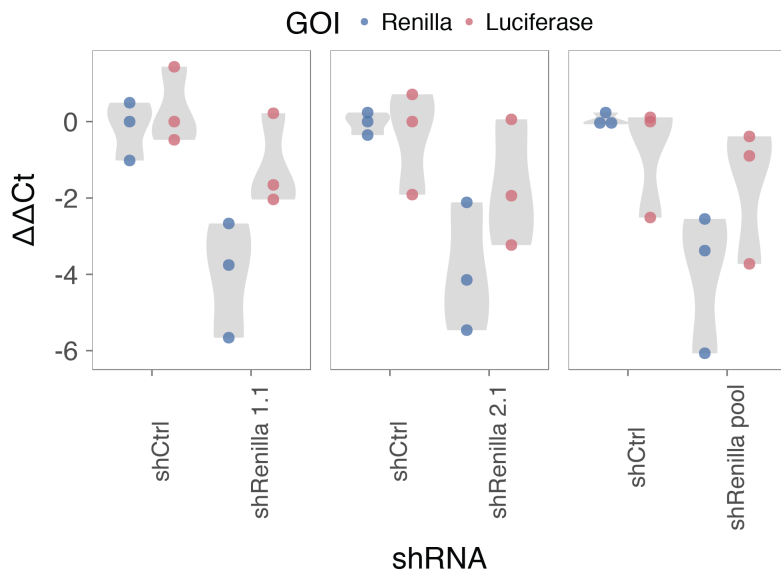


B)



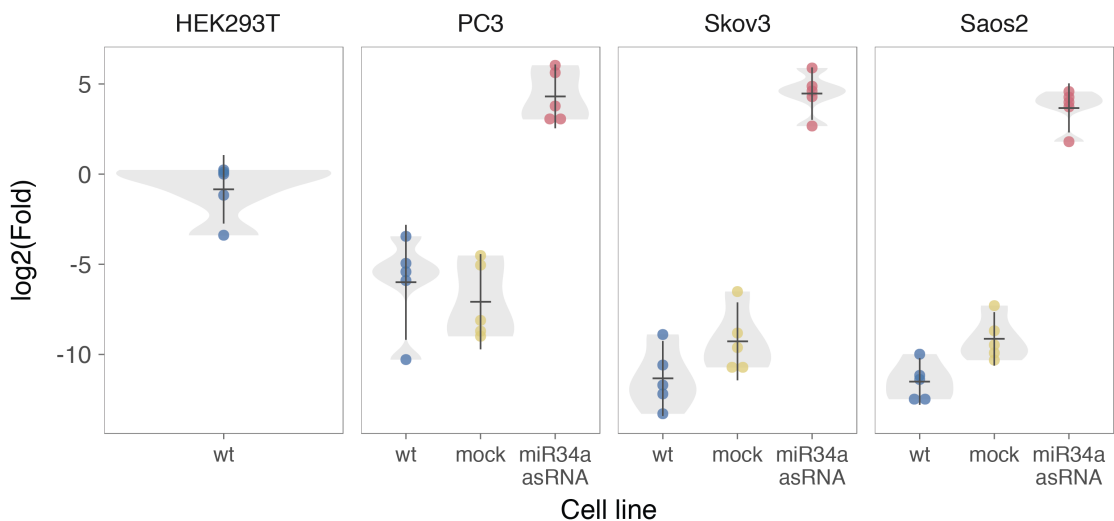
785
786
787
788
789
790

Figure 2 Supplement 1: A schematic representation of the p1 construct. A) A UCSC genome browser illustration indicating the location of the promoter region cloned into the p1 construct including the conserved *TP53*-binding site. **B)** A representative picture of the p1 construct including forward (F) and reverse (R) primer locations and the renilla shRNA targeting site.



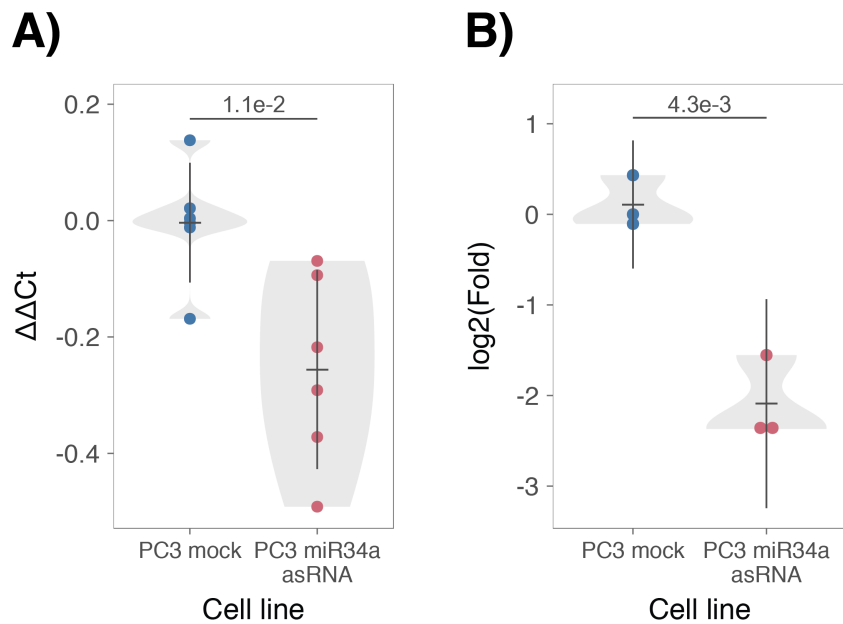
791
792
793
794
795
796
797

Figure 2 Supplement 2: Evaluating the effects of miR34a asRNA down-regulation. HEK293T cells were co-transfected with the p1 construct and either shRenilla or shControl. Renilla and luciferase levels were measured with Q-PCR 48 hours after transfection. Individual points represent independent experiments with the gray shadow indicating the density of the points. The experiment was performed in biological triplicate.



798
799

800 **Figure 3 Supplement 1: Physiological relevance of *miR34a* asRNA overexpression.** Comparison
801 of *miR34a* asRNA expression in HEK293T cells (high endogenous *miR34a* asRNA), and the wild-type
802 (wt), mock, and *miR34a* asRNA over-expressing stable cell lines.



803
804
805
806
807

Figure 3 Supplement 2: Effects of miR34a asRNA overexpression on cyclin D1. CCND1 expression (A) and western blot quantification of protein levels (B) in *miR34a* asRNA over-expressing PC3 stable cell lines. Experiments were performed in biological sextuplets (A) or triplicates (B).

808 **References**
809

- 810 Agostini, M., P. Tucci, R. Killick, E. Candi, B. S. Sayan, P. Rivetti di Val Cervo, P.
811 Nicotera, F. McKeon, R. A. Knight, T. W. Mak and G. Melino (2011). "Neuronal
812 differentiation by TAp73 is mediated by microRNA-34a regulation of synaptic
813 protein targets." *Proc Natl Acad Sci U S A* **108**(52): 21093-21098. DOI:
814 10.1073/pnas.1112061109
815
- 816 Ahn, Y. H., D. L. Gibbons, D. Chakravarti, C. J. Creighton, Z. H. Rizvi, H. P. Adams, A.
817 Pertsemlidis, P. A. Gregory, J. A. Wright, G. J. Goodall, E. R. Flores and J. M. Kurie
818 (2012). "ZEB1 drives prometastatic actin cytoskeletal remodeling by
819 downregulating miR-34a expression." *J Clin Invest* **122**(9): 3170-3183. DOI:
820 10.1172/JCI63608
821
- 822 Allaire, J., Y. Xie, J. McPherson, J. Luraschi, K. Ushey, A. Atkins, H. Wickham, J.
823 Cheng and W. Chang (2017). rmarkdown: Dynamic Documents for R. R package
824 version 1.8. <https://CRAN.R-project.org/package=rmarkdown>
825
- 826 Amarzguioui, M., J. J. Rossi and D. Kim (2005). "Approaches for chemically
827 synthesized siRNA and vector-mediated RNAi." *FEBS Lett* **579**(26): 5974-5981.
828 DOI: 10.1016/j.febslet.2005.08.070
829
- 830 Arnold, J. B. (2017). ggthemes: Extra Themes, Scales and Geoms for 'ggplot2'. R
831 package version 3.4.0. <https://CRAN.R-project.org/package=ggthemes>
832
- 833 Ashouri, A., V. I. Sayin, J. Van den Eynden, S. X. Singh, T. Papagiannakopoulos and
834 E. Larsson (2016). "Pan-cancer transcriptomic analysis associates long non-
835 coding RNAs with key mutational driver events." *Nature Communications* **7**:
836 13197. DOI: 10.1038/ncomms13197
837
- 838 Balbin, O. A., R. Malik, S. M. Dhanasekaran, J. R. Prensner, X. Cao, Y. M. Wu, D.
839 Robinson, R. Wang, G. Chen, D. G. Beer, A. I. Nesvizhskii and A. M. Chinnaian
840 (2015). "The landscape of antisense gene expression in human cancers." *Genome
841 Res* **25**(7): 1068-1079. DOI: 10.1101/gr.180596.114
842
- 843 Boque-Sastre, R., M. Soler, C. Oliveira-Mateos, A. Portela, C. Moutinho, S. Sayols, A.
844 Villanueva, M. Esteller and S. Guil (2015). "Head-to-head antisense transcription
845 and R-loop formation promotes transcriptional activation." *Proc Natl Acad Sci U
846 SA* **112**(18): 5785-5790. DOI: 10.1073/pnas.1421197112
847
- 848 Chang, T. C., D. Yu, Y. S. Lee, E. A. Wentzel, D. E. Arking, K. M. West, C. V. Dang, A.
849 Thomas-Tikhonenko and J. T. Mendell (2008). "Widespread microRNA
850 repression by Myc contributes to tumorigenesis." *Nat Genet* **40**(1): 43-50. DOI:
851 10.1038/ng.2007.30
852
- 853 Chang, W. (2014). extrafont: Tools for using fonts. R package version 0.17.
854 <https://CRAN.R-project.org/package=extrafont>
855

- 856 Chen, J., M. Sun, W. J. Kent, X. Huang, H. Xie, W. Wang, G. Zhou, R. Z. Shi and J. D.
857 Rowley (2004). "Over 20% of human transcripts might form sense-antisense
858 pairs." *Nucleic Acids Res* **32**(16): 4812-4820. DOI: 10.1093/nar/gkh818
- 859
- 860 Cheng, J., L. Zhou, Q. F. Xie, H. Y. Xie, X. Y. Wei, F. Gao, C. Y. Xing, X. Xu, L. J. Li and S.
861 S. Zheng (2010). "The impact of miR-34a on protein output in hepatocellular
862 carcinoma HepG2 cells." *Proteomics* **10**(8): 1557-1572. DOI:
863 10.1002/pmic.200900646
- 864
- 865 Chim, C. S., K. Y. Wong, Y. Qi, F. Loong, W. L. Lam, L. G. Wong, D. Y. Jin, J. F. Costello
866 and R. Liang (2010). "Epigenetic inactivation of the miR-34a in hematological
867 malignancies." *Carcinogenesis* **31**(4): 745-750. DOI: 10.1093/carcin/bgq033
- 868
- 869 Cole, K. A., E. F. Attiyeh, Y. P. Mosse, M. J. Laquaglia, S. J. Diskin, G. M. Brodeur and
870 J. M. Maris (2008). "A functional screen identifies miR-34a as a candidate
871 neuroblastoma tumor suppressor gene." *Mol Cancer Res* **6**(5): 735-742. DOI:
872 10.1158/1541-7786.MCR-07-2102
- 873
- 874 Conley, A. B. and I. K. Jordan (2012). "Epigenetic regulation of human cis-natural
875 antisense transcripts." *Nucleic Acids Res* **40**(4): 1438-1445. DOI:
876 10.1093/nar/gkr1010
- 877
- 878 Consortium, E. P. (2012). "An integrated encyclopedia of DNA elements in the
879 human genome." *Nature* **489**(7414): 57-74. DOI: 10.1038/nature11247
- 880
- 881 Ding, N., H. Wu, T. Tao and E. Peng (2017). "NEAT1 regulates cell proliferation
882 and apoptosis of ovarian cancer by miR-34a-5p/BCL2." *Onco Targets Ther* **10**:
883 4905-4915. DOI: 10.2147/OTT.S142446
- 884
- 885 Djebali, S., C. A. Davis, A. Merkel, A. Dobin, T. Lassmann, A. Mortazavi, A. Tanzer, J.
886 Lagarde, W. Lin, F. Schlesinger, C. Xue, G. K. Marinov, J. Khatun, B. A. Williams, C.
887 Zaleski, J. Rozowsky, M. Roder, F. Kokocinski, R. F. Abdelhamid, T. Alioto, I.
888 Antoshechkin, M. T. Baer, N. S. Bar, P. Batut, K. Bell, I. Bell, S. Chakrabortty, X.
889 Chen, J. Chrast, J. Curado, T. Derrien, J. Drenkow, E. Dumais, J. Dumais, R.
890 Duttagupta, E. Falconnet, M. Fastuca, K. Fejes-Toth, P. Ferreira, S. Foissac, M. J.
891 Fullwood, H. Gao, D. Gonzalez, A. Gordon, H. Gunawardena, C. Howald, S. Jha, R.
892 Johnson, P. Kapranov, B. King, C. Kingswood, O. J. Luo, E. Park, K. Persaud, J. B.
893 Preall, P. Ribeca, B. Risk, D. Robyr, M. Sammeth, L. Schaffer, L. H. See, A. Shahab, J.
894 Skancke, A. M. Suzuki, H. Takahashi, H. Tilgner, D. Trout, N. Walters, H. Wang, J.
895 Wrobel, Y. Yu, X. Ruan, Y. Hayashizaki, J. Harrow, M. Gerstein, T. Hubbard, A.
896 Reymond, S. E. Antonarakis, G. Hannon, M. C. Giddings, Y. Ruan, B. Wold, P.
897 Carninci, R. Guigo and T. R. Gingeras (2012). "Landscape of transcription in
898 human cells." *Nature* **489**(7414): 101-108. DOI: 10.1038/nature11233
- 899
- 900 Gallardo, E., A. Navarro, N. Vinolas, R. M. Marrades, T. Diaz, B. Gel, A. Quera, E.
901 Bandres, J. Garcia-Foncillas, J. Ramirez and M. Monzo (2009). "miR-34a as a
902 prognostic marker of relapse in surgically resected non-small-cell lung cancer."
903 *Carcinogenesis* **30**(11): 1903-1909. DOI: 10.1093/carcin/bgp219
- 904

- 905 Hunten, S., M. Kaller, F. Drepper, S. Oeljeklaus, T. Bonfert, F. Erhard, A. Dueck, N.
906 Eichner, C. C. Friedel, G. Meister, R. Zimmer, B. Warscheid and H. Hermeking
907 (2015). "p53-Regulated Networks of Protein, mRNA, miRNA, and lncRNA
908 Expression Revealed by Integrated Pulsed Stable Isotope Labeling With Amino
909 Acids in Cell Culture (pSILAC) and Next Generation Sequencing (NGS) Analyses."
910 Mol Cell Proteomics **14**(10): 2609-2629. DOI: 10.1074/mcp.M115.050237
- 911
- 912 International Human Genome Sequencing, C. (2004). "Finishing the euchromatic
913 sequence of the human genome." Nature **431**(7011): 931-945. DOI:
914 10.1038/nature03001
- 915
- 916 Johnsson, P., A. Ackley, L. Vidarsdottir, W. O. Lui, M. Corcoran, D. Grander and K.
917 V. Morris (2013). "A pseudogene long-noncoding-RNA network regulates PTEN
918 transcription and translation in human cells." Nat Struct Mol Biol **20**(4): 440-
919 446. DOI: 10.1038/nsmb.2516
- 920
- 921 Katayama, S., Y. Tomaru, T. Kasukawa, K. Waki, M. Nakanishi, M. Nakamura, H.
922 Nishida, C. C. Yap, M. Suzuki, J. Kawai, H. Suzuki, P. Carninci, Y. Hayashizaki, C.
923 Wells, M. Frith, T. Ravasi, K. C. Pang, J. Hallinan, J. Mattick, D. A. Hume, L. Lipovich,
924 S. Batalov, P. G. Engstrom, Y. Mizuno, M. A. Faghihi, A. Sandelin, A. M. Chalk, S.
925 Mottagui-Tabar, Z. Liang, B. Lenhard, C. Wahlestedt, R. G. E. R. Group, G. Genome
926 Science and F. Consortium (2005). "Antisense transcription in the mammalian
927 transcriptome." Science **309**(5740): 1564-1566. DOI: 10.1126/science.1112009
- 928
- 929 Kent, W. J., C. W. Sugnet, T. S. Furey, K. M. Roskin, T. H. Pringle, A. M. Zahler and D.
930 Haussler (2002). "The human genome browser at UCSC." Genome Res **12**(6):
931 996-1006. DOI: 10.1101/gr.229102. Article published online before print in May
932 2002
- 933
- 934 Kim, K. H., H. J. Kim and T. R. Lee (2017). "Epidermal long non-coding RNAs are
935 regulated by ultraviolet irradiation." Gene **637**: 196-202. DOI:
936 10.1016/j.gene.2017.09.043
- 937
- 938 Kong, L., Y. Zhang, Z. Q. Ye, X. Q. Liu, S. Q. Zhao, L. Wei and G. Gao (2007). "CPC:
939 assess the protein-coding potential of transcripts using sequence features and
940 support vector machine." Nucleic Acids Res **35**(Web Server issue): W345-349.
941 DOI: 10.1093/nar/gkm391
- 942
- 943 Lal, A., M. P. Thomas, G. Altschuler, F. Navarro, E. O'Day, X. L. Li, C. Concepcion, Y.
944 C. Han, J. Thiery, D. K. Rajani, A. Deutsch, O. Hofmann, A. Ventura, W. Hide and J.
945 Lieberman (2011). "Capture of microRNA-bound mRNAs identifies the tumor
946 suppressor miR-34a as a regulator of growth factor signaling." PLoS Genet **7**(11):
947 e1002363. DOI: 10.1371/journal.pgen.1002363
- 948
- 949 Leveille, N., C. A. Melo, K. Rooijers, A. Diaz-Lagares, S. A. Melo, G. Korkmaz, R.
950 Lopes, F. Akbari Moqadam, A. R. Maia, P. J. Wijchers, G. Geeven, M. L. den Boer, R.
951 Kalluri, W. de Laat, M. Esteller and R. Agami (2015). "Genome-wide profiling of
952 p53-regulated enhancer RNAs uncovers a subset of enhancers controlled by a
953 lncRNA." Nature Communications **6**: 6520. DOI: 10.1038/ncomms7520

954
955 Liu, C., K. Kelnar, B. Liu, X. Chen, T. Calhoun-Davis, H. Li, L. Patrawala, H. Yan, C.
956 Jeter, S. Honorio, J. F. Wiggins, A. G. Bader, R. Fagin, D. Brown and D. G. Tang
957 (2011). "The microRNA miR-34a inhibits prostate cancer stem cells and
958 metastasis by directly repressing CD44." *Nat Med* **17**(2): 211-215. DOI:
959 10.1038/nm.2284
960
961 Memczak, S., M. Jens, A. Elefsinioti, F. Torti, J. Krueger, A. Rybak, L. Maier, S. D.
962 Mackowiak, L. H. Gregersen, M. Munschauer, A. Loewer, U. Ziebold, M.
963 Landthaler, C. Kocks, F. le Noble and N. Rajewsky (2013). "Circular RNAs are a
964 large class of animal RNAs with regulatory potency." *Nature* **495**(7441): 333-
965 338. DOI: 10.1038/nature11928
966
967 O'Leary, N. A., M. W. Wright, J. R. Brister, S. Ciufo, D. Haddad, R. McVeigh, B.
968 Rajput, B. Robbertse, B. Smith-White, D. Ako-Adjei, A. Astashyn, A. Badretdin, Y.
969 Bao, O. Blinkova, V. Brover, V. Chetvernin, J. Choi, E. Cox, O. Ermolaeva, C. M.
970 Farrell, T. Goldfarb, T. Gupta, D. Haft, E. Hatcher, W. Hlavina, V. S. Joardar, V. K.
971 Kodali, W. Li, D. Maglott, P. Masterson, K. M. McGarvey, M. R. Murphy, K. O'Neill,
972 S. Pujar, S. H. Rangwala, D. Rausch, L. D. Riddick, C. Schoch, A. Shkeda, S. S. Storz,
973 H. Sun, F. Thibaud-Nissen, I. Tolstoy, R. E. Tully, A. R. Vatsan, C. Wallin, D. Webb,
974 W. Wu, M. J. Landrum, A. Kimchi, T. Tatusova, M. DiCuccio, P. Kitts, T. D. Murphy
975 and K. D. Pruitt (2016). "Reference sequence (RefSeq) database at NCBI: current
976 status, taxonomic expansion, and functional annotation." *Nucleic Acids Res*
977 **44**(D1): D733-745. DOI: 10.1093/nar/gkv1189
978
979 Ozsolak, F., P. Kapranov, S. Foissac, S. W. Kim, E. Fishilevich, A. P. Monaghan, B.
980 John and P. M. Milos (2010). "Comprehensive polyadenylation site maps in yeast
981 and human reveal pervasive alternative polyadenylation." *Cell* **143**(6): 1018-
982 1029. DOI: 10.1016/j.cell.2010.11.020
983
984 Polson, A., E. Durrett and D. Reisman (2011). "A bidirectional promoter reporter
985 vector for the analysis of the p53/WDR79 dual regulatory element." *Plasmid*
986 **66**(3): 169-179. DOI: 10.1016/j.plasmid.2011.08.004
987
988 Rashi-Elkeles, S., H. J. Warnatz, R. Elkon, A. Kupershtein, Y. Chobod, A. Paz, V.
989 Amstislavskiy, M. Sultan, H. Safer, W. Nietfeld, H. Lehrach, R. Shamir, M. L. Yaspo
990 and Y. Shiloh (2014). "Parallel profiling of the transcriptome, cistrome, and
991 epigenome in the cellular response to ionizing radiation." *Sci Signal* **7**(325): rs3.
992 DOI: 10.1126/scisignal.2005032
993
994 Raver-Shapira, N., E. Marciano, E. Meiri, Y. Spector, N. Rosenfeld, N. Moskovits, Z.
995 Bentwich and M. Oren (2007). "Transcriptional activation of miR-34a
996 contributes to p53-mediated apoptosis." *Mol Cell* **26**(5): 731-743. DOI:
997 10.1016/j.molcel.2007.05.017
998
999 Rinn, J. L., M. Kertesz, J. K. Wang, S. L. Squazzo, X. Xu, S. A. Brugmann, L. H.
1000 Goodnough, J. A. Helms, P. J. Farnham, E. Segal and H. Y. Chang (2007).
1001 "Functional demarcation of active and silent chromatin domains in human HOX

1002 loci by noncoding RNAs." *Cell* **129**(7): 1311-1323. DOI:
1003 10.1016/j.cell.2007.05.022
1004
1005 Rokavec, M., M. G. Oner, H. Li, R. Jackstadt, L. Jiang, D. Lodygin, M. Kaller, D. Horst,
1006 P. K. Ziegler, S. Schwitalla, J. Slotta-Huspenina, F. G. Bader, F. R. Greten and H.
1007 Hermeking (2015). "Corrigendum. IL-6R/STAT3/miR-34a feedback loop
1008 promotes EMT-mediated colorectal cancer invasion and metastasis." *J Clin Invest*
1009 **125**(3): 1362. DOI: 10.1172/JCI81340
1010
1011 Schneider, C. A., W. S. Rasband and K. W. Eliceiri (2012). "NIH Image to ImageJ:
1012 25 years of image analysis." *Nat Methods* **9**(7): 671-675.
1013
1014 Serviss, J. T. (2017). miR34AasRNaproject.
1015 https://github.com/GranderLab/miR34a_asRNA_project
1016
1017 Serviss, J. T., P. Johnsson and D. Grander (2014). "An emerging role for long non-
1018 coding RNAs in cancer metastasis." *Front Genet* **5**: 234. DOI:
1019 10.3389/fgene.2014.00234
1020
1021 Slabakova, E., Z. Culig, J. Remsik and K. Soucek (2017). "Alternative mechanisms
1022 of miR-34a regulation in cancer." *Cell Death Dis* **8**(10): e3100. DOI:
1023 10.1038/cddis.2017.495
1024
1025 Stahlhut, C. and F. J. Slack (2015). "Combinatorial Action of MicroRNAs let-7 and
1026 miR-34 Effectively Synergizes with Erlotinib to Suppress Non-small Cell Lung
1027 Cancer Cell Proliferation." *Cell Cycle* **14**(13): 2171-2180. DOI:
1028 10.1080/15384101.2014.1003008
1029
1030 Su, X., D. Chakravarti, M. S. Cho, L. Liu, Y. J. Gi, Y. L. Lin, M. L. Leung, A. El-Naggar,
1031 C. J. Creighton, M. B. Suraokar, I. Wistuba and E. R. Flores (2010). "TAp63
1032 suppresses metastasis through coordinate regulation of Dicer and miRNAs."
1033 *Nature* **467**(7318): 986-990. DOI: 10.1038/nature09459
1034
1035 Sun, F., H. Fu, Q. Liu, Y. Tie, J. Zhu, R. Xing, Z. Sun and X. Zheng (2008).
1036 "Downregulation of CCND1 and CDK6 by miR-34a induces cell cycle arrest."
1037 *FEBS Lett* **582**(10): 1564-1568. DOI: 10.1016/j.febslet.2008.03.057
1038
1039 Tarasov, V., P. Jung, B. Verdoodt, D. Lodygin, A. Epanchintsev, A. Menssen, G.
1040 Meister and H. Hermeking (2007). "Differential regulation of microRNAs by p53
1041 revealed by massively parallel sequencing: miR-34a is a p53 target that induces
1042 apoptosis and G1-arrest." *Cell Cycle* **6**(13): 1586-1593. DOI:
1043 10.4161/cc.6.13.4436
1044
1045 Team, R. C. (2017). "R: A Language and Environment for Statistical Computing."
1046 from <https://www.R-project.org/>.
1047
1048 Turner, A. M., A. M. Ackley, M. A. Matrone and K. V. Morris (2012).
1049 "Characterization of an HIV-targeted transcriptional gene-silencing RNA in
1050 primary cells." *Hum Gene Ther* **23**(5): 473-483. DOI: 10.1089/hum.2011.165

- 1051
1052 Vogt, M., J. Mundig, M. Gruner, S. T. Liffers, B. Verdoodt, J. Hauk, L.
1053 Steinstraesser, A. Tannapfel and H. Hermeking (2011). "Frequent concomitant
1054 inactivation of miR-34a and miR-34b/c by CpG methylation in colorectal,
1055 pancreatic, mammary, ovarian, urothelial, and renal cell carcinomas and soft
1056 tissue sarcomas." *Virchows Arch* **458**(3): 313-322. DOI: 10.1007/s00428-010-
1057 1030-5
1058
1059 Wang, L., P. Bu, Y. Ai, T. Srinivasan, H. J. Chen, K. Xiang, S. M. Lipkin and X. Shen
1060 (2016). "A long non-coding RNA targets microRNA miR-34a to regulate colon
1061 cancer stem cell asymmetric division." *eLife* **5**. DOI: 10.7554/eLife.14620
1062
1063 Wang, L., H. J. Park, S. Dasari, S. Wang, J. P. Kocher and W. Li (2013). "CPAT:
1064 Coding-Potential Assessment Tool using an alignment-free logistic regression
1065 model." *Nucleic Acids Res* **41**(6): e74. DOI: 10.1093/nar/gkt006
1066
1067 Wang, X., J. Li, K. Dong, F. Lin, M. Long, Y. Ouyang, J. Wei, X. Chen, Y. Weng, T. He
1068 and H. Zhang (2015). "Tumor suppressor miR-34a targets PD-L1 and functions
1069 as a potential immunotherapeutic target in acute myeloid leukemia." *Cell Signal*
1070 **27**(3): 443-452. DOI: 10.1016/j.cellsig.2014.12.003
1071
1072 Wickham, H. (2016). gtable: Arrange 'Grobs' in Tables. R package version 0.2.0.
1073 <https://CRAN.R-project.org/package=gtable>
1074
1075 Wickham, H. (2017). scales: Scale Functions for Visualization. R package version
1076 0.5.0. <https://CRAN.R-project.org/package=scales>
1077
1078 Wickham, H. (2017). tidyverse: Easily Install and Load the 'Tidyverse'. R package
1079 version 1.2.1. <https://CRAN.R-project.org/package=tidyverse>
1080
1081 Wickham, L. H. a. H. (2017). rlang: Functions for Base Types and Core R and
1082 'Tidyverse' Features. R package version 0.1.4. [https://CRAN.R-
1083 project.org/package=rlang](https://CRAN.R-project.org/package=rlang)
1084
1085 Wickham, S. M. B. a. H. (2014). magrittr: A Forward-Pipe Operator for R. R
1086 package version 1.5. <https://CRAN.R-project.org/package=magrittr>
1087
1088 Wilkins, D. gggenes: Draw Gene Arrow Maps in 'ggplot2'. R package version
1089 0.2.0.9003. <https://github.com/wilkox/gggenes>
1090
1091 Xiao, N. (2017). liftr: Containerize R Markdown Documents. R package version
1092 0.7. <https://CRAN.R-project.org/package=liftr>
1093
1094 Xie, Y. (2017). knitr: A General-Purpose Package for Dynamic Report Generation
1095 in R. R package version 1.17. <https://yihui.name/knitr/>
1096
1097 Yang, P., Q. J. Li, Y. Feng, Y. Zhang, G. J. Markowitz, S. Ning, Y. Deng, J. Zhao, S.
1098 Jiang, Y. Yuan, H. Y. Wang, S. Q. Cheng, D. Xie and X. F. Wang (2012). "TGF-beta-
1099 miR-34a-CCL22 signaling-induced Treg cell recruitment promotes venous

1100 metastases of HBV-positive hepatocellular carcinoma." *Cancer Cell* **22**(3): 291-
1101 303. DOI: 10.1016/j.ccr.2012.07.023
1102
1103 Yap, K. L., S. Li, A. M. Munoz-Cabello, S. Raguz, L. Zeng, S. Mujtaba, J. Gil, M. J.
1104 Walsh and M. M. Zhou (2010). "Molecular interplay of the noncoding RNA ANRIL
1105 and methylated histone H3 lysine 27 by polycomb CBX7 in transcriptional
1106 silencing of INK4a." *Mol Cell* **38**(5): 662-674. DOI: 10.1016/j.molcel.2010.03.021
1107
1108 Yu, W., D. Gius, P. Onyango, K. Muldoon-Jacobs, J. Karp, A. P. Feinberg and H. Cui
1109 (2008). "Epigenetic silencing of tumour suppressor gene p15 by its antisense
1110 RNA." *Nature* **451**(7175): 202-206. DOI: 10.1038/nature06468
1111
1112 Zenz, T., J. Mohr, E. Eldering, A. P. Kater, A. Buhler, D. Kienle, D. Winkler, J. Durig,
1113 M. H. van Oers, D. Mertens, H. Dohner and S. Stilgenbauer (2009). "miR-34a as
1114 part of the resistance network in chronic lymphocytic leukemia." *Blood* **113**(16):
1115 3801-3808. DOI: 10.1182/blood-2008-08-172254
1116
1117
1118
1119